CORTEX 132 (2020) 238–249

Available online at www.sciencedirect.com

ScienceDirect

Journal homepage: www.elsevier.com/locate/cortex

Single Case Report

Network-level causal analysis of set-shifting during trail making test part B: A multimodal analysis of a glioma surgery case

Emmanuel Mandonnet [a,b,c,*], *Marion Vincent* [d,e], *Antoni Valero-Cabré* [c,f], *Valentine Facque* [a,c], *Marion Barberis* [a], *François Bonnetblanc* [e], *François Rheault* [f], *Emmanuelle Volle* [c], *Maxime Descoteaux* [g,1] *and Daniel S. Margulies* [c,1]

[a] *Department of Neurosurgery, Lariboisière Hospital, APHP, Paris, France*
[b] *University Paris 7, Paris, France*
[c] *Frontlab, CNRS UMR 7225, Inserm U1127, Sorbonne Université ICM, Paris, France*
[d] *University of Lille, CNRS, CHU Lille, UMR 9193, SCALab – Affectives and Cognitives Sciences Lab, Lille, France*
[e] *INRIA, University of Montpellier, LIRMM, CAMIN Team, Montpellier, France*
[f] *Cognitive Neuroscience and Information Technology Research Program, Open University of Catalonia (UOC), Barcelona, Catalunya, Spain*
[g] *Sherbrook Connectivity Imaging Lab, Department of Computer Science, Faculty of Sciences, Université de Sherbrook, Sherbrook, Canada*

ARTICLE INFO

Article history:
Received 9 March 2020
Reviewed 11 May 2020
Revised 18 May 2020
Accepted 24 August 2020
Action editor Sarah MacPherson
Published online 12 September 2020

ABSTRACT

The trail making test part B (TMT-B) is one of the most widely used task for the assessment of set-shifting ability in patients. However, the set of brain regions impacting TMT-B performance when lesioned is still poorly known. In this case report, we provide a multimodal analysis of a patient operated on while awake for a diffuse low-grade glioma located in the right supramarginal gyrus. TMT-B performance was probed intraoperatively. Direct electrical stimulation of the white matter in the depth of the resection generated shifting errors. Using the recent methodology of axono-cortical-evoked potentials (ACEP), we demonstrated that the eloquent fibers were connected to the posterior end of the middle temporal gyrus (MTG). This was further confirmed by a tractography analysis of the postoperative diffusion MRI. Finally, the functional connectivity maps of this MTG seed were assessed in both pre- and post-operative resting state MRI. These maps matched with the Control network B (13th) and Default B (17th) from the 17-networks parcellation of (Yeo et al., 2011). Last but not least, we showed that the dorsal attention B (6th), the control A & B networks (12th and 13th) and the default A (16th) have been preserved here but disconnected after a more extensive resection in a previous glioma case within the same area, and in whom TMT-B was definitively impaired. Taken together, these data support the

* *Corresponding author*. Hôpital Lariboisière, 2 rue Ambroise Paré, 75010, Paris, France.
E-mail address: mandonnet@mac.com (E. Mandonnet).
[1] These authors contributed equally to this work.
https://doi.org/10.1016/j.cortex.2020.08.021

need of a network-level approach to identify the neural basis of the TMT-B and point to the Control network B as playing an important role in set-shifting.

1. Introduction

Awake surgery with motor and language mapping under direct electrical stimulation is currently the gold standard method to achieve maximal resection while preserving motor and language functions (De Witt Hamer et al., 2012). Over the past decade, several teams applied this methodology to monitor - especially when operating in the right hemisphere - other functions than motricity and language, including, but not limited to, spatial awareness, non-verbal semantics, emotion recognition, or mentalizing (see (Vilasboas et al., 2017) for a review). However, very few reports focused on the monitoring of executive functions, which seems surprising given the importance of such abilities in daily life. To the best of our knowledge, two groups studied the inhibition component, by making use of an intraoperative version of the Stroop task (Puglisi et al., 2018; Wager et al., 2013), one group studied spatial working memory (Kinoshita et al., 2016), while set-shifting was never investigated in this context. The part B of the trail making test (TMT-B) - consisting to join in ascending order, and alternatively, numbers and letters randomly distributed over a sheet of paper - is a simple way to explore set-shifting abilities in a patient. Despite the fact that several areas implicated in set-shifting of TMT-B have been identified by functional imaging studies in healthy individuals and lesion-mapping studies in stroke patients (see (Varjacic et al., 2018) for a recent review), we still lack a clear picture of how these different areas could be linked together to form a network.

Recently, we reported the case of a patient who endured a definitive impairment of the TMT-B after surgical resection of a right temporo-parietal glioma (Mandonnet et al., 2017). Even after several months of cognitive rehabilitation, this patient was unable to perform the TMT-B. We demonstrated that this deficit was associated with changes in both structural and functional connectivity. The absence of the right fronto-temporo-parietal network in the postoperative resting-state fMRI data was corroborated by the resection, which mapped to the long direct segment of arcuate fasciculus, the first branch of the posterior transverse system (see new nomenclature proposed in (Mandonnet et al., 2018), i.e., the posterior vertical branch of arcuate fasciculus according to standard terminology), the third branch of superior longitudinal fasciculus, and the callosal fibers.

In the present paper, we analyze a second case with a surgical resection of a glioma located in the very same area (see Fig. 1). We combined several modalities in order to further clarify the neural correlates of the changes in performance on TMT-B: intraoperative causal evaluation of TMT-B with direct electrical stimulation at the cortical and axonal levels, intra-operative recordings of axono-cortical evoked-potentials, postoperative structural connectivity based on diffusion-weighted imaging (DWI), and pre- and post-operative resting state functional connectivity.

2. Methods

We report all data exclusions (if any), all inclusion/exclusion criteria, whether inclusion/exclusion criteria were established prior to data analysis, all manipulations, and all measures in the study.

2.1. Ethics statement

Patient gave full informed consent to participate to this study, which was approved by the ethics committee of Saint-Louis hospital (reference 2013/51). No part of the study procedures nor part of the study analyses were pre-registered in a time-stamped, institutional registry prior to the research being conducted. The conditions of our ethics approval do not permit public archiving of patient data. Readers seeking access to the data should contact the lead author EM. Access will be granted to named individuals in accordance with ethical procedures governing the reuse of sensitive data (no specific conditions).

2.2. Clinical case

A 53 years old right-handed man without any previous medical history was diagnosed using MRI with a right parietal diffuse low-grade glioma (see Fig. 1), revealed by a generalized seizure. After a short period of follow-up confirming the slow evolution of the tumor, the patient underwent a surgical resection in awake condition, as described below. Resection was complete (see Fig. 1) and there were no neurological complications. He could resume work four months after surgery.

2.3. Diffusion-weighted imaging

Diffusion-weighted imaging (DWI) was acquired immediately pre- and 4-months post-surgery. A 3T Siemens Skyra system (Siemens, Erlangen, Germany) with a 64-channel phased-array head coil, was employed to acquire DWI of the whole head with an anterior-posterior phase of acquisition. DWI parameters consisted in an acquisition matrix of $108 \times 108 \times 120$ voxels of 2.3 mm^3 with a total field of view of $250 \times 250 \times 120$ mm^3. DWI was acquired along 64 directions

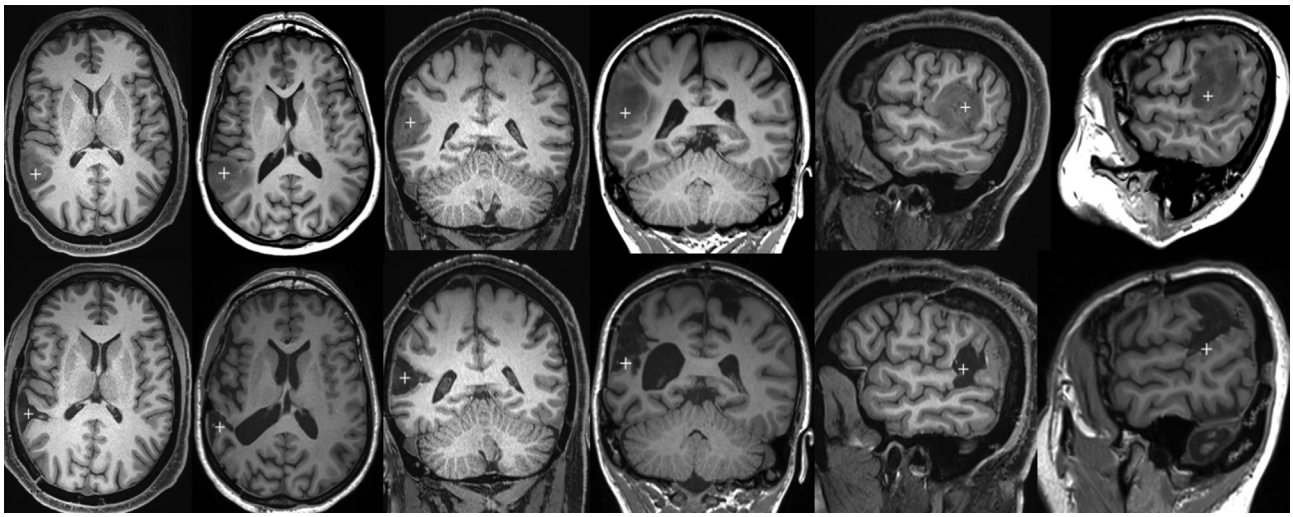

Fig. 1 – Comparison of tumor location and resection between the present case and our previously published one (Mandonnet et al., 2017). Top: preoperative 3D-T1. Bottom: postoperative 3D-T1. For each orientation, the present case is on the left, and the previous one on the right.

with a weighting b = 2000 s/mm^2. Additionally, non-weighted (b = 0) volumes were also acquired. Echo Time (TE) was set at 95 msec and Repetition Time (TR) at 7700 msec. The whole sequence lasted 9min45sec.

2.4. *Resting state functional magnetic resonance imaging (rs-fMRI)*

rs-fMRI was acquired immediately pre- and 4-months post-surgery. During scanning, the participant was instructed to rest, but to remain awake with his eyes closed. A gradient echo planar imaging (EPI) sequence was used to acquire 130 volumes (94 × 94 × 36 voxels, 2.1 × 2.1 × 3 mm^3, and a field of view of 200 × 200 × 108 mm^3). The TR was 3200 msec and the TE was 30 msec. The total rs-fMRI scan lasted 7 min.

2.5. *Cognitive testing*

Pre-operative and postoperative long-term (4 months) testing assessed the following cognitive domains (Mandonnet et al., 2015):

- Language functions, including naming 80 black & white pictures (DO 80) (Metz-Lutz et al., 1991), and literal and categorical word fluencies,
- Non-verbal semantic association, using the Pyramids and Palm Trees Test (PPTT) (Howard & Patterson, 1992)
- Visuo-spatial abilities: copy of Rey figure (Rey, 1941)
- Memory: forward and backward digital span, verbal span, free and cued selective 16-items reminding test (Grober et al., 1988); delayed copy of Rey figure
- Attention: d2 attention test (Brickenkamp, 1981)
- Spatial awareness: Bell's test, line bisection (Thiebaut de Schotten et al., 2005)
- Executive functions: Stroop test (Stroop, 1935), Trail making test part A & B (Godefroy et al., 2010), Paced Auditory Serial Addition Test (PASAT) (Gronwall, 1977)

All of these tests were administered by pen and paper and are not available in electronic form.

2.6. *Intraoperative monitoring*

Surgery was performed in awake condition, following the same methodology as previously reported (Mandonnet et al., 2015). Based on the location of the tumor, spatial awareness was continuously tested with an electronic tablet version of the line bisection test (Thiebaut de Schotten et al.; 2005; Vallar et al.; 2014*b*). This also allowed to monitor continuously sensori-motor abilities of the left upper limb, as the patient had to point the middle of the line on the tablet with his left finger. The PPTT was also regularly checked, with the aim to detect the parietal terminations of the inferior longitudinal system (Herbet et al., 2017). Finally, based on the previous patient's deficit after resection of a tumor in a similar location (Mandonnet et al., 2017), the TMT-B was also implemented as an electronic tablet version and monitored during surgery. In this electronic tablet version, numbers and letters were distributed semi-randomly, in such a way that a linear path could be tracked by linking alternatively numbers and letters (see video in supplementary file S1). The software plotted the line between the previous and current items only if the patient pointed the right item on the tablet with his left finger. Hence, errors could not be marked nor recorded as a wrong line on the tablet. Resection was pushed further until a site was found as eloquent for a given test, that is if disturbances were consistently generated in at least two consecutive trials under active stimulation. The patient was video-recorded during the whole awake testing period. The patient camera was synchronized with the camera recording the operative field and with the video of the electronic tablet on which the tasks were presented.

Supplementary video related to this article can be found at https://doi.org/10.1016/j.cortex.2020.08.021

2.7. Axono-cortical evoked potentials recordings

At the end of the tumor resection, the axonal site found to be eloquent when probed with 60 Hz stimulation was stimulated at a frequency of 1 Hz. In both cases, constant-current biphasic square pulses (single pulse duration of 500 μs) were delivered with certified intra-operative stimulation equipment (Nimbus iCare light, Innopsys, Narbonne, France) by means of a bipolar stimulation probe (two straight 1 mm diameter electrode tips with a pitch of 5 mm, forming a "Y") kept in direct contact with brain tissue. This site location was registered with the MRI-based neuronavigation system (S7, Medtronic, Minnesota, USA). Stimulation intensity was set at 3 mA, i.e., the same at which 60 Hz stimulation was found effectively interfering with function during mapping. Two sets of 1 min recordings were obtained, as the surgeon rotated by 180° the stimulation probe, thus inverting the polarity of the stimulation pulses, in order to wash out responses caused by the stimulus artefact (Vincent et al., 2017). Two strips of 6 electrodes each (Dixi medical, Chaudefontaine, France, diameter = 2.5 mm, inter-electrode distance = 1 cm) were placed over the middle temporal gyrus (MTG) (electrodes 1–6) and the lateral part of the intraparietal sulcus (electrodes 7–12). Electrodes 1–6 were recorded using a differential montage (1–2, 3–4, 5–6), while electrodes 7–12 were recorded in a referential montage (with a reference electrode placed on the left mastoid bone). A common ground electrode was placed on the right scapular bone. Cortical potentials were recorded using continuous electro-corticography (ISIS-IOM, and InomedGmbH, Emmendingen, Germany). Digitalized datasets (sampling rate = 2000 Hz, amplitude coding = 16 bits, bandpass filter of .5 Hz–4000 Hz, 50 Hz-notch filter) were analyzed offline by a custom-made Matlab script (written by MV) (Mathworks, Natick, Massachusetts, USA). Prestimulus baseline was determined by averaging over 75 ms before the stimulus onset for each of the evoked potentials. This offset was then subtracted for each potential, thus normalizing each pre-stimulus potential to zero. Potentials were then averaged time-locked to the electrical pulse onset.

2.8. Tractography

Tractograms were obtained using a home-made pipeline (written by FR). From the b = 2000 s/mm^2 volumes, fiber orientation distribution function (fODF) was estimated using constrained spherical deconvolution (CSD) (Descoteaux et al., 2007; Tournier et al., 2007). Probabilistic tractography (Descoteaux et al., 2009; Tournier et al., 2012) was subsequently computed with 10^6 initial seeds, in order to make sure that sufficient density and spatial coverage were achieved, resulting in 739,546 streamlines. Seeding and tracking masks were obtained by thresholding the FA map at .10. Most computational tools were provided by the Dipy library (Garyfallidis et al., 2014).

2.9. Functional connectivity

rs-fMRI data were preprocessed using the Configurable Pipeline for the Analysis of Connectomes (C-PAC) ('Frontiers | Towards Automated Analysis of Connectomes', n.d.). Both pre- and post-scans were processed independently using the standard pipelines, which included motion correction, nuisance regression using CompCor, and nonlinear registration to MNI152 template space. Seed-based functional connectivity analysis was conducted by correlating all voxels with the average time-series from within the region-of-interest (ROI). Results were Fisher's f-to-z transformed and smoothed using a 6 mm Gaussian kernel (FWHM). For visualization purposes, individual-level functional connectivity maps were thresholded at >.15 and cluster volume >20 mm^3. Comparison of the thresholded functional connectivity maps with the 17 networks of (Yeo et al., 2011) was conducted by calculating the Dice coefficient between each pair of maps.

2.10. Network-level disconnection analysis ("Disconets")

The principle is to compute quantitatively how much the surgical cavity disconnected each of Yeo's networks (Yeo et al., 2011). Twenty (20) whole-brain tractograms of the 7T Human Connectome Project (HCP) subjects (see supplementary file S8 for the subjects' IDs) were used in MNI space as an atlas-based representation of connections in a healthy brain. Tractograms were produced using constrained-spherical deconvolution deterministic tractography with Starstrack (https://www.mr-startrack.com), as detailed in (Karolis et al., 2019). Each of Yeo's 17-networks was used, separately, as a mask to filter tractograms of each of the 20 healthy HCP subjects (selecting streamlines with "both ends" within each network), using an home-made routine, based on SCILPY tools (https://github.com/scilus/scilpy). Then, the manually extracted segmentation of the surgical cavity mask (put in the MNI space using ANTs registration, https://github.com/ANTsX/ANTs) was used to further filter the previous tractograms (selecting those streamlines with "any part" within the surgical cavity). A "disconnection score" was computed for each subject and for each network as [(Track-count within network − Track-count within lesion)/Track-count within network] * 100, and then averaged over the 20 subjects.

3. Results

3.1. Intraoperative monitoring

The cortical mapping identified a site in the post–central gyrus (see Fig. 2, tag 2), whose stimulation at 3 mA generated an arrest of the counting task, without stopping a repetitive voluntary arm movement. On the cortical surface, no sites were found to induce disturbances of the PPTT, the line bisection, or the TMT-B. In the depth, at the level of the sagittal stratum, the patient was monitored continuously with TMT-B and the resection was pursued as long as no errors were detected, whether spontaneously or under stimulation (see first part of video in supplementary file S1). At some point, 3 mA stimulation generated an impossibility to shift from digits to letters in the TMT-B (tag 4 on

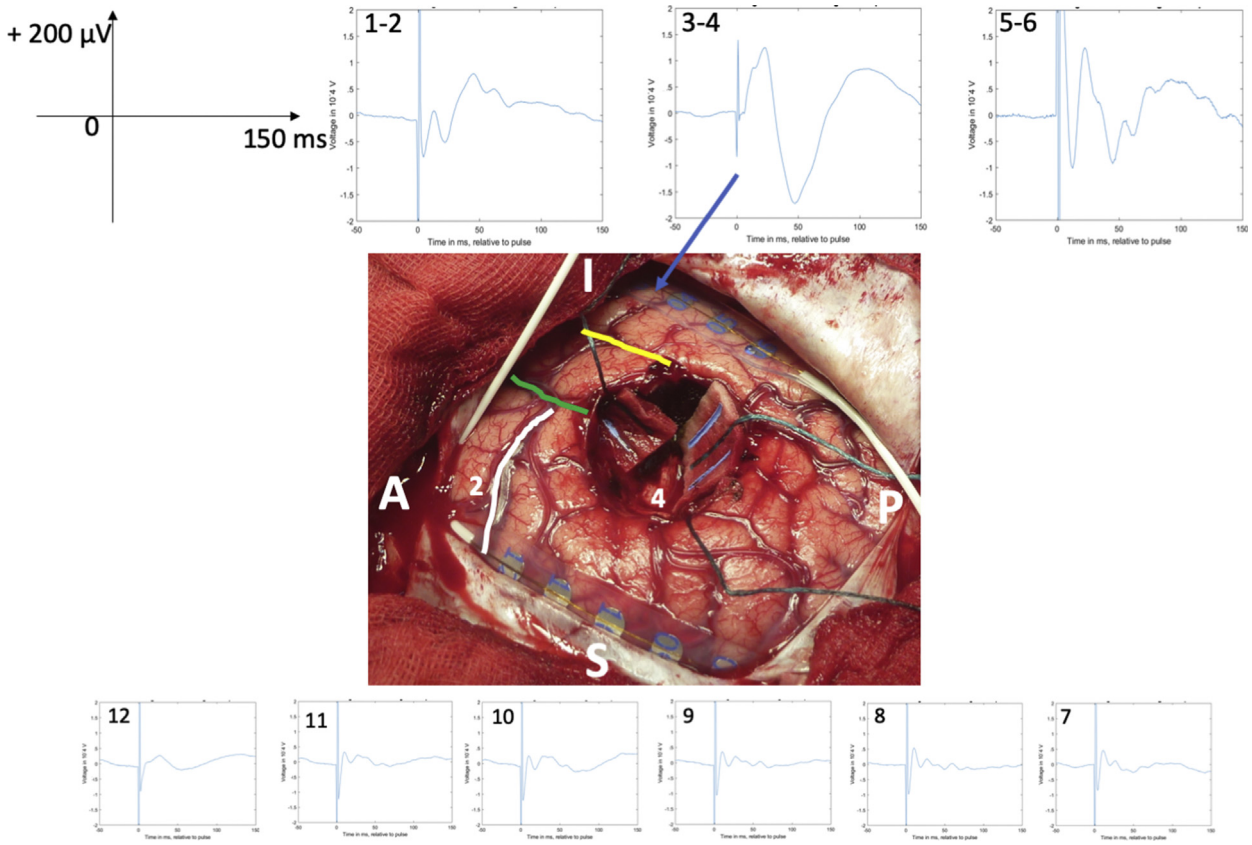

Fig. 2 – Intraoperative photography of the mapping and electrophysiological recordings. The stimulation of the site labeled by the cortical tag 2 elicited an arrest of counting. The axonal tag 4 corresponds to the stimulation site where the patient failed to shift from numbers to letters in the TMT-B (see video in supplementary file S1). Surface potentials were recorded when stimulating site 4 at 3 mA, at a frequency of 1 Hz. White line: postcentral sulcus, Green line: lateral fissure, Yellow line: superior temporal sulcus.

intraoperative photography on Fig. 2) on two consecutive stimulation trials: on the first one, he skipped the letter 'A', going from the '1' to the '2', and on the second one - and after a period without any stimulation during which the patient performed successfully – he skipped the letter 'D', going from the '4' to the '5' (see video showing this second stimulation trial). These errors prompted the surgeon to stop the resection (whereas in a previous case report of a patient with a similar location but without TMT-B monitoring during the surgery, the resection was pushed further up to the ventricle ependyma (Mandonnet et al., 2017)). On the second stimulation trial, the patient was unaware of his error: after selecting number '4', he persisted in pointing to number '5', despite the fact that this wrong response could not be selected. Even once the stimulation was stopped, the patient continued to ignore letters, and pointed to number '6' (despite the fact that the track from '4' to '5' was not drawn on the tablet). After a couple of seconds and with the help of the speech therapist who said "not the '6', be careful, what was the last ?", he suddenly resumed the task appropriately, saying "A, B, C, D, the '4' with the 'D', the '5' with the 'E', the '6' with the 'F', …", while pointing to the correct items on the tablet.

This site 4 defined our seed for analysis of postoperative tractogram. Of note, as in the previous case, no disruption of PPTT nor of line bisection was found during the whole intraoperative monitoring.

3.2. *Cognitive outcomes*

The full preoperative, immediate- and late-postoperative cognitive evaluations are presented in Table 1. Pre-operative evaluation revealed mild signs of left spatial neglect in the Rey Figure copy, a reduced processing speed in auditory-verbal attention task (PASAT), and a significant impairment of visual attention d2-task (that could be partly attributed to decreased visual acuity, in keeping with sequelae of a cytomegalovirus meningitis at the age of 15). TMT-B was correctly performed: no errors and normal speed. Immediate postoperative performances were similar with pre-operative scores. However, two scores were slightly lower postoperatively compared to pre-operatively: the difference TMT-B – TMT-A (+.2 SD preop, –.1 SD immediately postop) and the PASAT (39/60 (–1.7 SD) preop, 30/60 (–2.9 SD) immediately postop). Four months later, all performances were similar or better than before the surgery. In particular, the

Table 1 – Pre- and post-operative results of cognitive evaluations.

		Preoperative scores	Immediate postoperatives scores	Postoperative scores
Language	DO80	80 (.9)	80 (.9)	80 (.9)
	LWF	20 (.4)	19 (−.1)	22 (.3)
	CWF	31 (.4)	34 (.7)	25 (−.4)
	PPTT	50 (.3)	50 (.3)	51 (.73)
Praxies (Rey figure copy)	Planning	IV	I	I
	Score	30 (−4.2)	36 (.8)	34 (−.8)
Memory	Forward span	6 (.2)	5 (−.7)	5 (−.7)
	Backward span	4 (−.3)	3 (−1.2)	4 (−.3)
	VEM	16:9 (−1.3): 15	–	16:14 (1): 16
	Delayed Rey	18 (−.7)	–	25 (.3)
Spatial awareness	Bell's test omissions	2 (0)	0 (1)	1 (.5)
	Line bisection	−8 mm	−11,5 mm	−5.5 mm
Attention& Executive functions	PASAT	39 (−1.7)	30 (−2.9)	55 (.4)
	TMT-B	95" (.1)	96" (.1)	85" (.3)
	TMT B-A	53" (.2)	62" (−.1)	46" (.4)
	Stroop-c	133" (−.6)	98" (.7)	107" (.4)
	d2 - KL	48	116	127
Processing speed	TMT A	42'' (−.1)	33''88 (.3)	39" (.1)
	Rey	2'16 (.9)	–	2'04 (1)
	Stroop-n	54" (.6)	63" (−.1)	39" (0,1)
	d2-GZ	340	275	321

Numbers between brackets correspond to the standard deviations to average. LWF = literal word fluency, CWF = categorical word fluency, PPTT = Pyramids and Palm Trees Test, VEM = verbal explicit memory (sum of free and cued recall and total delayed recall are separated by a double dots), VIM = Visual Implicit Memory (scores set 1 & 2); PASAT = paced auditory serial addition test, TMT B-A = difference in timing of the trail making test part B & part A, Stroop-c = difference in timing of the conflict and rectangle color naming tasks, d2-KL = score KL of the d2 attention test, Rey = time to copy, Stroop-n = timing to name the colors of the rectangles, d2-GZ = score GZ of d2 attention test.

patient improved his score at the TMT-B (from 95'' (.1 SD) preoperatively to 85'' (.3 SD) postoperatively) and at the PASAT (from 39/60 (−1.7 SD) preoperatively to 55/60 (.4 SD)).

3.3. *Tractography*

We placed an 8 mm ROI on the postoperative MRI at the site whose stimulation impaired TMT-B (see tag 4 on Fig. 2, MNI coordinates of the center of the ROI: x = 38, y = −42, z = 12). To be as accurate as possible, we used the intraoperative snapshot of the neuronavigation (see Supplementary Fig. S2). This ROI was used as a seed to virtually dissect the post-operative tractogram, allowing to show the fibers passing through the stimulation site 4 (see Fig. 3). These fibers included parts of the arcuate fasciculus, the middle longitudinal fasciculus, the inferior longitudinal system (using the nomenclature recently published in (Mandonnet et al., 2018), i.e., inferior fronto-occipital fasciculus according to the standard terminology), and the corpus callosum (See Fig. S3). Importantly, the branches of the arcuate fasciculus ended in the middle temporal gyrus (MTG) (see Fig. 3), while none of them reached the lateral part of the intraparietal sulcus (IPS). We defined a MTG tractography ROI (see yellow ROI on Fig. 3) at the location where fibers terminated in the MTG, in order to subsequently compare this ROI with another one located where ACEPs were recorded when stimulating white matter site 4 (see below).

Finally, we put manually onto the MNI atlas a 8 mm ROI, corresponding to the site 4. As described in a previous study of our group (Corrivetti et al., 2019), we considered this ROI as a lesion for the Tractotron software (Foulon et al., 2018). Results are given in Table 2 and are in agreement with our

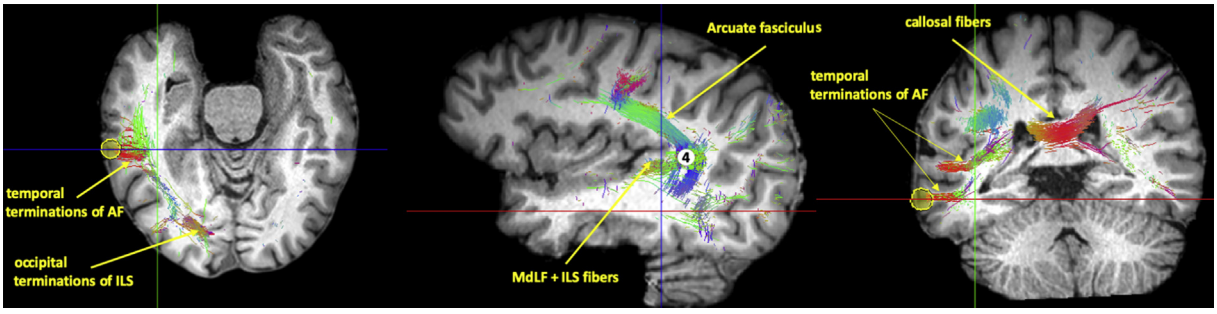

Fig. 3 – Postoperative tractography. The seed was a 8-mm ROI located at the stimulation site. The yellow 8-mm sphere corresponds to the termination of the fibers in the middle temporal gyrus.

Table 2 – Probabilities of tracts disconnection by the electrical stimulation.

Tract	Probability
Arcuate_Posterior_Segment_Right	1.000000
Corpus_callosum	.984000
Inferior_Longitudinal_Right	.944000
Inferior_Fronto_Occipital_fasciculus_Right	.880000
Arcuate_Long segment_Right	.860000
Superior_Longitudinal Fasciculus_III_Right	.800000
Optic_Radiations_Right	.664000
Arcuate_Anterior_Segment_Right	.260000
Anterior_Commissure	.256000
Superior_Longitudinal Fasciculus_II_Right	.240000

The probabilities were provided by the Tractotron analysis, using a 8 mm ROI located at the white matter stimulation site.

virtual dissections (given the fact that, in the Tractotron, the tract named "inferior longitudinal fasciculus" also includes the fibers that we assigned to the middle longitudinal fasciculus and that the tract named "superior longitudinal fasciculus III" also includes the fibers that we assigned to the arcuate fasciculus). One difference was noted: the posterior part of the arcuate fasciculus (also called "posterior transverse system" in the new nomenclature (Mandonnet et al., 2018)) could not be identified in the postoperative tractogram whereas it was seen in the preoperative tractogram (see Fig. S4), suggesting that this tract was removed by the surgical resection.

3.4. *Electrophysiological recordings*

ACEPs were recorded on the electrodes placed over the MTG (see Fig. 2, electrodes 1 to 6), whereas none could be detected over the lateral part of the IPS (electrodes 7 to 12). The ACEP with the highest amplitude was recorded between electrodes 3 & 4, with a baseline to peak amplitude of 173 μV and a latency (pulse onset to ACEP peak) of 48 ms.

3.5. *Comparison between electrophysiology and tractography*

Qualitatively, our electrophysiological recordings (i.e., ACEP recorded only in the strip covering the MTG) were in agreement with our tractography results. To go a step further in the comparison, we first defined a MTG ACEP ROI, by locating on the preoperative 3D-T1 with gadolinium injection the position of the electrodes where we recorded a highest amplitude ACEP. To this end, we reconstructed the 3D surface of the brain from this image, allowing to make a good visual comparison with the intraoperative photography (see Supplementary Fig. S5), as explained in (Corrivetti et al., 2019). We thus placed an 8-mm ROI on the preoperative T1 in a location that matched the position of the MTG electrodes 3 & 4. We then used the FLIRT algorithm to transform the MTG tractography ROI (indicated in yellow on Fig. 3) in the preoperative T1 space. The two resulting ACEP - and tractography-based ROIs were overlaid on the preoperative T1 with MRIcroGL, showing a good overlap (see Fig. 4).

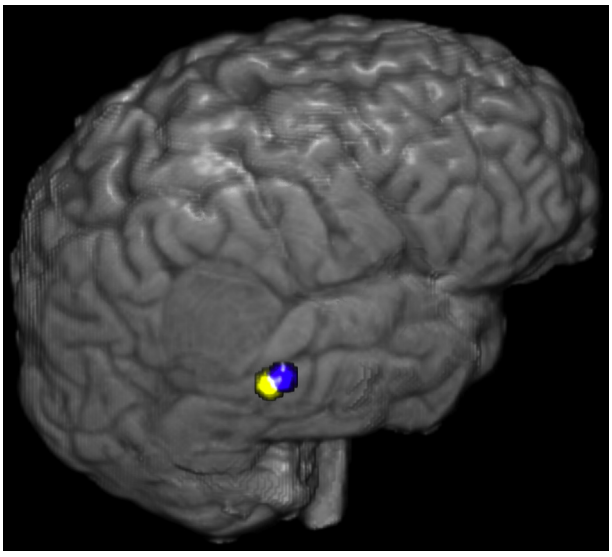

Fig. 4 – Agreement between tractography and electrophysiological recordings. The yellow ROI corresponds to cortical terminations in middle temporal gyrus of tractogram fibers passing through the stimulation site '4'. The blue ROI corresponds to the position of the electrodes where the highest amplitude ACEP was recorded. Background image corresponds to the patient's T1 image.

3.6. *Functional connectivity of the site of highest amplitude ACEP*

We first projected the 17 resting state networks proposed by (Yeo et al., 2011) in healthy individuals onto the patient's MRI space (see Fig. 5). The ACEP-based MTG ROI overlapped with the *Control network B* (13th in the 17-network parcellation, at its junction with the 17th, named Default B, see nomenclature in (Shinn et al., 2015)). The control network B clearly co-localizes with the fronto-parieto-temporal network whose connectivity was found to be postoperatively impaired in our previously published case (see Fig. S6 and (Mandonnet et al., 2017) for further details).

Functional connectivity analysis of the patient rs-fMRI data using as a seed the ACEP-based MTG ROI revealed a pattern that qualitatively overlapped with the 13th and 17th network observed in the healthy control analysis (see Fig. 5). While the pre-op network had notably higher functional connectivity than the post-op one, the functionally connected regions remained homologous. Quantitatively, the overlap between healthy control Yeo's parcellation and patient's functional connectivity of the MTG ROI was clearly higher for the 13th and 17th networks, both for pre- and post-operative resting states (see Fig. S7).

3.7. *Network-level disconnection analysis*

The percentages of disconnection by the surgical cavity for each network of Yeo's 17-parcellation are given in Table 3. For the present patient-case, the most disconnected network was the network 14, all other network being less than 5%

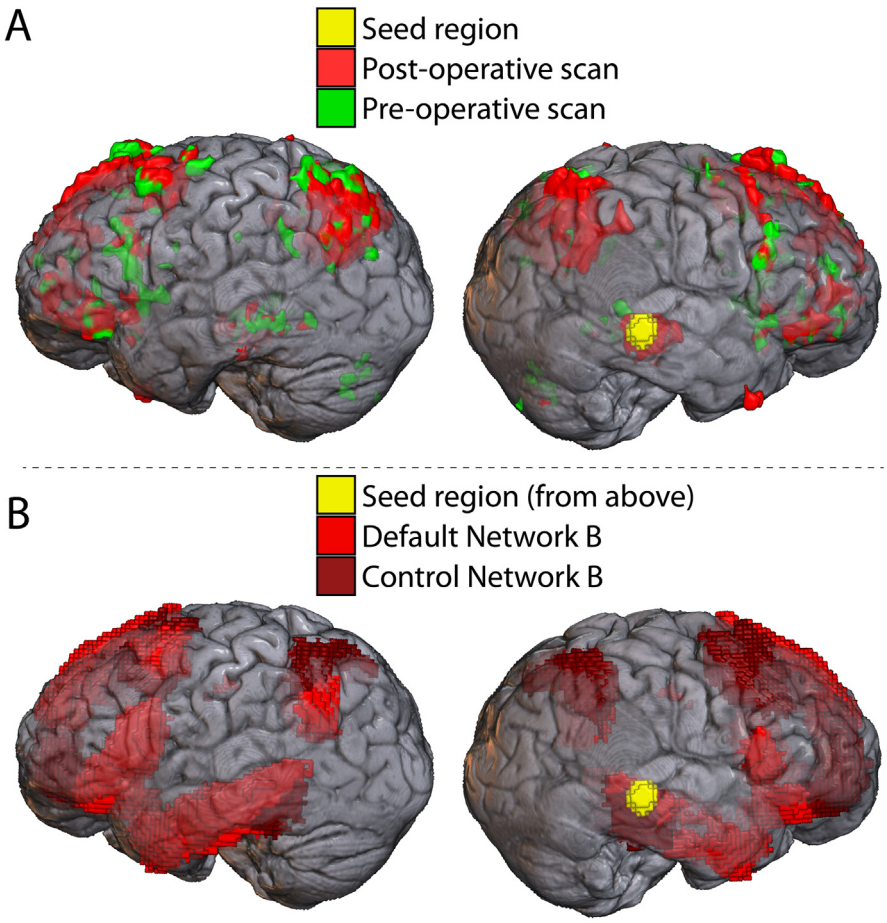

Fig. 5 – Patient's own functional connectivity from a seed region located at cortical site where the highest amplitude ACEP was recorded. A: The pre-operative functional connectivity map is represented in red, and the post-operative in green. B: For comparison, the Control B and Default B network maps (from the 17 networks of Yeo et al., 2011) are projected onto the patient's brain. These two networks demonstrated the highest overlap among all 17 networks (see Fig. S7). The seed region (yellow) is presented for comparison to the network locations.

disconnected. For the previous patient-case, network 14, 6, 13, 7, 12 were the most disconnected (percentages = 25, 13.3, 9.2, 8.9, 7.6). Finally, we also computed for the present patient-case the percentages of disconnection when adding to the surgical cavity the 8 mm ROI corresponding to the white matter stimulation site of tag 4: the addition of this 8 mm ROI to the surgical cavity specifically increased the disconnection of networks 12, 13, 16.

4. Discussion

We here showed an intraoperative impairment on TMT-B performance during the transient disruption of white matter fibers passing through the right parieto-temporal junction, suggesting the causal contribution of this white matter area in set-shifting as assessed by TMT-B.

Importantly, intraoperative identification of the fibers eliciting errors in the TMT-B preserved the patient's ability to perform the TMT-B: his postoperative scores were similar to the preoperative scores. We interpret these findings in comparison with our previously reported case, in whom TMT-B was not monitored during electrical mapping and in whom a more extensive resection led to completely impaired performance of the TMT-B postoperatively. Hence, the present case suggests that intraoperative monitoring of TMT-B could help to preserve set-shifting abilities when performing a surgical resection in this region, a proposal that awaits further confirmation in a larger series of patients, as recommended in (Mandonnet et al., 2020).

Importantly, the agreement between the tractograms and the ACEP, pointing to a common node in the MTG, co-validates the two methods. Separately, each of those methods comes with limitations, especially in a single case. While the limitations of tractography are well-known (see for example (Maier-Hein et al., 2017)), the reliability of axono-cortical evoked potentials has been less studied, given the novelty of this methodology. False positives could have been generated by the amplifier response to the stimulus artefact (Vincent et al., 2017) or confounded by source localization issues (Boyer et al., 2020; Shimada et al., 2017). Both warnings have been checked in the present case: ACEPs were similar whatever the polarity of the initial phase of the biphasic pulse, and the recording in differential montage puts strong spatial

Table 3 – Network-level disconnection induced by the surgical cavity (current case and previous case) and the surgical cavity + the 8 mm ROI of electrical stimulation.

	Current case (%)		Previous case (%)
	Surgical cavity	Surgical cavity + stimulated ROI	Surgical cavity
1 (visual peripheral)	0	.02	0
2 (visual central)	0	0	0
3 (somato-motor A)	0	0	1.29
4 (somato-motor B)	1.25	1.3	5.5
5 (dorsal attention A)	0	.3	.59
6 (dorsal attention B)	0	.3	**13.31**
7 (ventral attention)	4.3	4.3	**8.9**
8 (salience)	.86	.86	1.51
9 (limbic)	0	0	.01
10 (limbic)	0	0	0
11 (control C)	0	0	0
12 (control A)	.16	**1.6**	**7.6**
13 (control B)	.62	**1.9**	**9.2**
14 (default D – auditory)	10.16	14.75	25.3
15 (default C)	0	0	.23
16 (default A)	.13	**.5**	**5.44**
17 (default B)	.05	.09	.16

Higher indices of disconnection are given in bold.

constraints regarding source localization. Finally, we think the convergence of the two results is important to mention and can trigger further group studies to confirm such findings.

Furthermore, our evoked potential, structural connectivity and functional connectivity explorations allowed us to determine that the electrical stimulus propagated across a fronto-parieto-temporal network, a system whose connectivity was shown to be damaged in our previously published case (Mandonnet et al., 2017). Though often referred to as the fronto-parietal control network (Smith et al., 2009), it is worth emphasizing that this network also includes a node in the MTG of the temporal lobe, as pictured in the 17-parcellation of Yeo (see Fig. S7). Thus, the involvement of this MTG area in set-shifting abilities would deserve further investigations through neuroimaging and lesion-mapping studies. We also acknowledge that we did not record evoked activity over the whole right hemisphere, given both the limited extent of the craniotomy and the limited number of electrodes at our disposal. Moreover, it was not possible to reach the contralateral hemisphere with ECoG electrodes (scalp EEG could eventually provide approximations to such contralaterally evoked activity, but the spatial resolution would be poor compared to intracranial ECoG). Hence, due to these limitations, we cannot conclude whether evoked activity could have been observed in areas lying outside the resting state network found from a seed in the MTG ROI. Nonetheless, the good overlap between the functional connectivity of the MTG ROI and the Control B (13th) and Default B (17th) networks fits well with a previous study demonstrating that performance in cognitive flexibility correlated with the dynamic functional connectivity between the control and default networks of the 7-networks parcellation (Douw et al., 2016).

From a neuropsychological perspective, the present work has several limitations, due in part to the constraints imposed by the intraoperative settings. In particular, we could not fully dissect which cognitive (sub)processes were impaired when the patient failed to shift. However, PPTT and line bisection acted as control tasks, showing that the patient had no spatial neglect nor any non-verbal semantic disorder. Furthermore, the patient appeared capable of picking up, in correct ascending order, the numbers '4', '5', '6', suggesting that he was able to select one category of items in correct order, but could not alternate numbers with letters. Moreover, it cannot be ruled out that the behavioral disturbance could have been generated by remote afterdischarges to other areas, as no electrophysiological recordings were performed while stimulating at 60 Hz. However, while such phenomenon have been reported for cortical stimulation (Ishitobi et al., 2000), it has never been described, to the best of our knowledge, for white matter stimulation.

Nevertheless, the present work provides another piece of the puzzle to the complex problem of integrating in a wider framework the different regions found to impact the TMT-B task across several lesion studies. As recently reviewed (Varjacic et al., 2018), a great variety of areas have been associated to TMT-B in lesion studies (Anderson et al., 1995; Barbey et al., 2012; Demakis, 2004; Gläscher et al., 2012; Kopp et al., 2015; MacPherson et al., 2015; Miskin et al., 2016; Muir et al., 2015; Stuss et al., 2001; Varjačić et al., 2018), including, but not limited to, the left rostral anterior cingulate (Gläscher et al., 2012), the left dorsomedial prefrontal cortex (Miskin et al., 2016), the left insular cortex and nearby white matter of external capsule (Varjačić et al., 2018), the right dorsolateral prefrontal cortex (Kopp et al., 2015), the left superior longitudinal fasciculus and lateral cholinergic pathways (Muir et al., 2015). Many factors can account for this diversity: selection of different pathologies and/or at different stages (acute *vs* chronic), selection of different

outcome measures or scores (time TMT-B, time difference TMT-B − TMT-A, shifting errors, sequencing errors, …), analysis bias towards frontal locations (for example, retrospectively, the right temporo-parietal junction is not discussed by (Barbey et al., 2012; Gläscher et al., 2012), albeit evidenced in their results), and inherent limitations of voxels-lesion symptoms mapping (Mah et al., 2014) that considers lesion location but overlooks network functioning. The present case, combined with the previously published one by our team (Mandonnet et al., 2017), allows us to put forward a tentative hypothesis: performance at the TMT-B (either time difference TMT-B − TMT-A or number of errors) should be better explained by looking at the degree of disconnection within several networks, and our new "Disconets" methodology pointed to control B (13th network) (together with dorsal attention B, control A, and default A- respectively 6th, 12th, and 16th networks) as differentially disconnected by the resection in the previous patient-case compared to current patient-case and differentially disconnected by electrical stimulation in the current patient-case. Of note, the degree of disconnection of 14th network (default D − auditory), is more difficult to interpret, as it is constituted of a unique large area within the superior temporal gyrus, and its disconnection is quite high in both patient-cases. Such an hypothesis could be tested in future studies by determining over a larger series of patients the predictive value of these network disconnection indices regarding the long-term performance in TMT-B.

Author contribution

Emmanuel Mandonnet: Conceptualization; Data curation; Formal analysis; Funding acquisition; Methodology; Supervision; Visualization; Writing - original draft; Marion Vincent: Data curation; Formal analysis; Writing − review & editing; Antoni Valero-Cabré: Data curation; Writing - original draft; Valentine Facque: Data curation; Writing − review & editing; Marion Barberis: Data curation; Writing − review & editing; François Bonnetblanc: Data curation; Writing − review & editing; François Rheault: Software; Writing − review & editing; Emmanuelle Volle: Writing − review & editing; Maxime Descoteaux: Formal analysis; Software; Writing − review & editing; Daniel S. Margulies: Formal analysis; Methodology; Supervision; Visualization; Writing - original draft.

Funding

This work was partly funded by the CRC chirurgie-2016 from AP-HP. EM is also supported by the Contrat Interface 2018 from INSERM.

Acknowledgements

EM thanks Michel Thiebaut de Schotten for having provided the tractograms of the 20 HCP subjects used in the Disconets.

Supplementary data

Supplementary data to this article can be found online at https://doi.org/10.1016/j.cortex.2020.08.021.

REFERENCES

Anderson, C. V., Bigler, E. D., & Blatter, D. D. (1995). Frontal lobe lesions, diffuse damage, and neuropsychological functioning in traumatic brain-injured patients. *Journal of Clinical and Experimental Neuropsychology, 17*(6), 900–908. https://doi.org/10.1080/01688639508402438

Barbey, A. K., Colom, R., Solomon, J., Krueger, F., Forbes, C., & Grafman, J. (2012). An integrative architecture for general intelligence and executive function revealed by lesion mapping. *Brain: A Journal of Neurology, 135*(Pt 4), 1154–1164. https://doi.org/10.1093/brain/aws021

Boyer, A., Ramdani, S., Duffau, H., Dali, M., Vincent, M., Mandonnet, M., Guiraud, D., & Bonnetblanc, F. (2020). Electrophysiological mapping during brain tumor surgery: a new insight into the human brain connectivity. *Brain Topography*. Submitted.

Brickenkamp, R. (1981). *Test d2: Aufmerksamkeits-Belastungs-Test (Test d2: Concentration-Endurance Test: Manual)*. Verlag fur Psychologie.

Corrivetti, F., de Schotten, M. T., Poisson, I., Froelich, S., Descoteaux, M., Rheault, F., & Mandonnet, E. (2019). Dissociating motor-speech from lexico-semantic systems in the left frontal lobe: insight from a series of 17 awake intraoperative mappings in glioma patients. *Brain Structure & Function, 224*(3), 1151–1165. https://doi.org/10.1007/s00429-019-01827-7

De Witt Hamer, P. C., Robles, S. G., Zwinderman, A. H., Duffau, H., & Berger, M. S. (2012). Impact of intraoperative stimulation brain mapping on glioma surgery outcome: a meta-analysis. *Journal of Clinical Oncology: Official Journal of the American Society of Clinical Oncology, 30*(20), 2559–2565. https://doi.org/10.1200/JCO.2011.38.4818

Demakis, G. J. (2004). Frontal lobe damage and tests of executive processing: a meta-analysis of the category test, stroop test, and trail-making test. *Journal of Clinical and Experimental Neuropsychology, 26*(3), 441–450. https://doi.org/10.1080/13803390490510149

Descoteaux, M., Angelino, E., Fitzgibbons, S., & Deriche, R. (2007). Regularized, fast, and robust analytical Q-ball imaging. *Magnetic Resonance in Medicine, 58*(3), 497–510. https://doi.org/10.1002/mrm.21277

Descoteaux, M., Deriche, R., Knösche, T. R., & Anwander, A. (2009). Deterministic and probabilistic tractography based on complex fibre orientation distributions. *IEEE Transactions on Medical Imaging, 28*(2), 269–286. https://doi.org/10.1109/TMI.2008.2004424

Douw, L., Wakeman, D. G., Tanaka, N., Liu, H., & Stufflebeam, S. M. (2016). State-dependent variability of dynamic functional connectivity between frontoparietal and default networks relates to cognitive flexibility. *Neuroscience, 339*, 12–21. https://doi.org/10.1016/j.neuroscience.2016.09.034

Foulon, C., Cerliani, L., Kinkingnéhun, S., Levy, R., Rosso, C., Urbanski, M., Volle, E., & Thiebaut de Schotten, M. (2018). Advanced lesion symptom mapping analyses and implementation as BCBtoolkit. *GigaScience, 7*(3), 1–17. https://doi.org/10.1093/gigascience/giy004

Frontiers. Towards automated analysis of connectomes: The Configurable Pipeline for the Analysis of Connectomes (C-PAC)

(n.d.). Retrieved April 24, 2019, from: https://www.frontiersin.org/10.3389/conf.fninf.2013.09.00042/event_abstract.
Garyfallidis, E., Brett, M., Amirbekian, B., Rokem, A., van der Walt, S., Descoteaux, M., & Nimmo-Smith, I. (2014). Dipy, a library for the analysis of diffusion MRI data. *Frontiers in Neuroinformatics, 8*. https://doi.org/10.3389/fninf.2014.00008
Gläscher, J., Adolphs, R., Damasio, H., Bechara, A., Rudrauf, D., Calamia, M., Paul, L. K., & Tranel, D. (2012). Lesion mapping of cognitive control and value-based decision making in the prefrontal cortex. *Proceedings of the National Academy of Sciences of the United States of America, 109*(36), 14681–14686. https://doi.org/10.1073/pnas.1206608109
Godefroy, O., Azouvi, P., Robert, P., Roussel, M., LeGall, D., Meulemans, T., & Groupe de Réflexion sur l'Evaluation des Fonctions Exécutives Study Group. (2010). Dysexecutive syndrome: diagnostic criteria and validation study. *Annals of Neurology, 68*(6), 855–864. https://doi.org/10.1002/ana.22117
Grober, E., Buschke, H., Crystal, H., Bang, S., & Dresner, R. (1988). Screening for dementia by memory testing. *Neurology, 38*(6), 900–903.
Gronwall, D. M. (1977). Paced auditory serial-addition task: a measure of recovery from concussion. *Perceptual and Motor Skills, 44*(2), 367–373. https://doi.org/10.2466/pms.1977.44.2.367
Herbet, G., Moritz-Gasser, S., & Duffau, H. (2017). Direct evidence for the contributive role of the right inferior fronto-occipital fasciculus in non-verbal semantic cognition. *Brain Structure & Function, 222*(4), 1597–1610. https://doi.org/10.1007/s00429-016-1294-x
Howard, D., & Patterson, K. (1992). *The Pyramids and Palm Trees Test: A Test for Semantic Access From Words and Pictures*. Bury St. Edmunds: Thames Valley Test Company.
Ishitobi, M., Nakasato, N., Suzuki, K., Nagamatsu, K., Shamoto, H., & Yoshimoto, T. (2000). Remote discharges in the posterior language area during basal temporal stimulation. *Neuroreport, 11*(13), 2997–3000. https://doi.org/10.1097/00001756-200009110-00034
Karolis, V. R., Corbetta, M., & Thiebaut de Schotten, M. (2019). The architecture of functional lateralisation and its relationship to callosal connectivity in the human brain. *Nature Communications, 10*(1), 1417. https://doi.org/10.1038/s41467-019-09344-1
Kinoshita, M., Nakajima, R., Shinohara, H., Miyashita, K., Tanaka, S., Okita, H., Nakada, M., & Hayashi, Y. (2016). Chronic spatial working memory deficit associated with the superior longitudinal fasciculus: a study using voxel-based lesion-symptom mapping and intraoperative direct stimulation in right prefrontal glioma surgery. *Journal of Neurosurgery, 125*(4), 1024–1032. https://doi.org/10.3171/2015.10.JNS1591
Kopp, B., Rösser, N., Tabeling, S., Stürenburg, H. J., de Haan, B., Karnath, H.-O., & Wessel, K. (2015). Errors on the trail making test are associated with right hemispheric frontal lobe damage in stroke patients. *Behavioural Neurology, 2015*, 309235. https://doi.org/10.1155/2015/309235
MacPherson, S. E., Della Sala, S., Cox, S. R., Girardi, A., & Iveson, M. H. (2015). *Handbook of Frontal Lobe Assessment (DRAFT)*. Oxford University Press. http://www.oxfordclinicalpsych.com/view/10.1093/med:psych/9780199669523.001.0001/med-9780199669523.
Mah, Y.-H., Husain, M., Rees, G., & Nachev, P. (2014). Human brain lesion-deficit inference remapped. *Brain: A Journal of Neurology, 137*(Pt 9), 2522–2531. https://doi.org/10.1093/brain/awu164
Maier-Hein, K. H., Neher, P. F., Houde, J.-C., Côté, M.-A., Garyfallidis, E., Zhong, J., Chamberland, M., Yeh, F.-C., Lin, Y.-C., Ji, Q., Reddick, W. E., Glass, J. O., Chen, D. Q., Feng, Y., Gao, C., Wu, Y., Ma, J., Renjie, H., Li, Q., … Descoteaux, M. (2017). The challenge of mapping the human connectome based on diffusion tractography. *Nature Communications, 8*(1), 1349. https://doi.org/10.1038/s41467-017-01285-x
Mandonnet, E., Cerliani, L., Siuda-Krzywicka, K., Poisson, I., Zhi, N., Volle, E., & de Schotten, M. T. (2017). A network-level approach of cognitive flexibility impairment after surgery of a right temporo-parietal glioma. *Neuro-Chirurgie, 63*(4), 308–313. https://doi.org/10.1016/j.neuchi.2017.03.003
Mandonnet, E., De Witt Hamer, P., Poisson, I., Whittle, I., Bernat, A.-L., Bresson, D., Madadaki, C., Bouazza, S., Ursu, R., Carpentier, A. F., George, B., & Froelich, S. (2015). Initial experience using awake surgery for glioma: oncological, functional, and employment outcomes in a consecutive series of 25 cases. *Neurosurgery, 76*(4), 382–389. https://doi.org/10.1227/NEU.0000000000000644. discussion 389.
Mandonnet, E., Herbet, G., & Duffau, H. (2020). Letter: Introducing new tasks for intraoperative mapping in awake glioma surgery: Clearing the line between patient care and scientific research. *Neurosurgery, 86*(2), E256–E257. https://doi.org/10.1093/neuros/nyz447
Mandonnet, E., Sarubbo, S., & Petit, L. (2018). The nomenclature of human white matter association pathways: Proposal for a systematic taxonomic anatomical classification. *Frontiers in Neuroanatomy, 12*, 94. https://doi.org/10.3389/fnana.2018.00094
Metz-Lutz, M., Kremin, H., Deloche, G., Hannequin, D., Ferrand, L., & Perrier, D. (1991). Standardisation d'un test de dénomination orale: Contrôle des effets de l'âge, du sexe et du niveau de scolarité chez les sujets adultes normaux. *Review in Neuropsychology, 1*, 73–95.
Miskin, N., Thesen, T., Barr, W. B., Butler, T., Wang, X., Dugan, P., Kuzniecky, R., Doyle, W., Devinsky, O., & Blackmon, K. (2016). Prefrontal lobe structural integrity and trail making test, part B: Converging findings from surface-based cortical thickness and voxel-based lesion symptom analyses. *Brain Imaging and Behavior, 10*(3), 675–685. https://doi.org/10.1007/s11682-015-9455-8
Muir, R. T., Lam, B., Honjo, K., Harry, R. D., McNeely, A. A., Gao, F.-Q., Ramirez, J., Scott, C. J. M., Ganda, A., Zhao, J., Zhou, X. J., Graham, S. J., Rangwala, N., Gibson, E., Lobaugh, N. J., Kiss, A., Stuss, D. T., Nyenhuis, D. L., Lee, B.-C., … Black, S. E. (2015). Trail making test elucidates neural substrates of specific poststroke executive dysfunctions. *Stroke; a Journal of Cerebral Circulation, 46*(10), 2755–2761. https://doi.org/10.1161/STROKEAHA.115.009936
Puglisi, G., Sciortino, T., Rossi, M., Leonetti, A., Fornia, L., Conti Nibali, M., Casarotti, A., Pessina, F., Riva, M., Cerri, G., & Bello, L. (2018). Preserving executive functions in nondominant frontal lobe glioma surgery: an intraoperative tool. *Journal of Neurosurgery*, 1–7. https://doi.org/10.3171/2018.4.JNS18393
Rey, A. (1941). L'examen psychologique dans les cas d'encéphalopathie traumatique. *Arch Psychol, 28*, 328–336.
Shimada, S., Kunii, N., Kawai, K., Matsuo, T., Ishishita, Y., Ibayashi, K., & Saito, N. (2017). Impact of volume-conducted potential in interpretation of cortico-cortical evoked potential: Detailed analysis of high-resolution electrocorticography using two mathematical approaches. *Clinical Neurophysiology: Official Journal of the International Federation of Clinical Neurophysiology, 128*(4), 549–557. https://doi.org/10.1016/j.clinph.2017.01.012
Shinn, A. K., Baker, J. T., Lewandowski, K. E., Öngür, D., & Cohen, B. M. (2015). Aberrant cerebellar connectivity in motor and association networks in schizophrenia. *Frontiers in Human Neuroscience, 9*, 134. https://doi.org/10.3389/fnhum.2015.00134
Smith, S. M., Fox, P. T., Miller, K. L., Glahn, D. C., Fox, P. M., Mackay, C. E., Filippini, N., Watkins, K. E., Toro, R., Laird, A. R., & Beckmann, C. F. (2009). Correspondence of the brain's functional architecture during activation and rest. *Proceedings*

of the National Academy of Sciences of the United States of America, 106(31), 13040–13045. https://doi.org/10.1073/pnas.0905267106

Stroop, J. (1935). Studies of interference in serial verbal reactions. *J Exp Psychol, 6*, 643–662.

Stuss, D. T., Bisschop, S. M., Alexander, M. P., Levine, B., Katz, D., & Izukawa, D. (2001). The trail making test: A study in focal lesion patients. *Psychological Assessment, 13*(2), 230–239.

Thiebaut de Schotten, M., Urbanski, M., Duffau, H., Volle, E., Lévy, R., Dubois, B., & Bartolomeo, P. (2005a). Direct evidence for a parietal-frontal pathway subserving spatial awareness in humans. *Science (New York, N.Y.), 309*(5744), 2226–2228. https://doi.org/10.1126/science.1116251

Tournier, J.-D., Calamante, F., & Connelly, A. (2007). Robust determination of the fibre orientation distribution in diffusion MRI: non-negativity constrained super-resolved spherical deconvolution. *NeuroImage, 35*(4), 1459–1472. https://doi.org/10.1016/j.neuroimage.2007.02.016

Tournier, J.-D., Calamante, F., & Connelly, A. (2012). MRtrix: Diffusion tractography in crossing fiber regions. *International Journal of Imaging Systems and Technology, 22*(1), 53–66. https://doi.org/10.1002/ima.22005

Vallar, G., Bello, L., Bricolo, E., Castellano, A., Casarotti, A., Falini, A., Riva, M., Fava, E., & Papagno, C. (2014). Cerebral correlates of visuospatial neglect: a direct cerebral stimulation study. *Human Brain Mapping, 35*(4), 1334–1350. https://doi.org/10.1002/hbm.22257

Varjacic, A., Mantini, D., Demeyere, N., & Gillebert, C. R. (2018). Neural signatures of Trail Making Test performance: Evidence from lesion-mapping and neuroimaging studies. *Neuropsychologia, 115*, 78–87. https://doi.org/10.1016/j.neuropsychologia.2018.03.031

Varjačić, A., Mantini, D., Levenstein, J., Slavkova, E. D., Demeyere, N., & Gillebert, C. R. (2018). The role of left insula in executive set-switching: Lesion evidence from an acute stroke cohort. *Cortex; a Journal Devoted to the Study of the Nervous System and Behavior, 107*, 92–101. https://doi.org/10.1016/j.cortex.2017.11.009

Vilasboas, T., Herbet, G., & Duffau, H. (2017). Challenging the myth of right nondominant hemisphere: Lessons from corticosubcortical stimulation mapping in awake surgery and surgical implications. *World Neurosurgery, 103*, 449–456. https://doi.org/10.1016/j.wneu.2017.04.021

Vincent, M., Guiraud, D., Duffau, H., Mandonnet, E., & Bonnetblanc, F. (2017). Electrophysiological brain mapping: Basics of recording evoked potentials induced by electrical stimulation and its physiological spreading in the human brain. *Clinical Neurophysiology: Official Journal of the International Federation of Clinical Neurophysiology, 128*(10), 1886–1890. https://doi.org/10.1016/j.clinph.2017.07.402

Wager, M., Du Boisgueheneuc, F., Pluchon, C., Bouyer, C., Stal, V., Bataille, B., Guillevin, C. M., & Gil, R. (2013). Intraoperative monitoring of an aspect of executive functions: administration of the Stroop test in 9 adult patients during awake surgery for resection of frontal glioma. *Neurosurgery, 72*(2 Suppl Operative), ons169–ons180. https://doi.org/10.1227/NEU.0b013e31827bf1d6. discussion ons180-181.

Yeo, B. T. T., Krienen, F. M., Sepulcre, J., Sabuncu, M. R., Lashkari, D., Hollinshead, M., Roffman, J. L., Smoller, J. W., Zöllei, L., Polimeni, J. R., Fischl, B., Liu, H., & Buckner, R. L. (2011). The organization of the human cerebral cortex estimated by intrinsic functional connectivity. *Journal of Neurophysiology, 106*(3), 1125–1165. https://doi.org/10.1152/jn.00338.2011